



# Defect sensitivity mitigation in the compressive mechanical response of two-phase lattice metamaterials

Matteo Montanari, Roberto Brighenti, Andrea Spagnoli \*

Department of Engineering and Architecture, University of Parma, Parco Area delle Scienze 181/A, 43124 Parma, Italy

## ARTICLE INFO

### Keywords:

Metamaterials  
Lattice structures  
Additive manufacturing  
Defect mitigation

## ABSTRACT

Engineered materials commonly referred to as *metamaterials* are materials that offer appealing features such as customisable stiffness and strength, auxetic behaviour and energy absorption. This work focuses on the classical 2D lattice metamaterial configuration with regular triangular unit cell. A combination of two dissimilar materials is employed in the design process: the *primary* material that constitutes the lattice structure is composed of thermoplastic polyurethane (TPU), while an incompressible silicone serves as the *secondary* material, completely filling selected lattice cells. In order to investigate the mechanical response of such lattices to intrinsic defects, geometric imperfections are intentionally introduced. Three distinct types of geometric anomalies, i.e. curvature of some elements, lateral shift of some lattice nodes, and reduced beam thickness, are randomly introduced. Additively manufactured perfect and defective lattices are subjected to compressive loading for both empty and silicone filled cases. Overall, the results reveal that the lattices show a significant improvement with the assumed reinforcing filling pattern, helping to prevent the buckling of the beams under compression and enhancing the load bearing capacity of the structure at higher deformations. Finite element (FE) analyses are performed to validate the experimental results, demonstrating how the filling pattern enhances the mechanical response of the lattices.

## 1. Introduction

Periodic metamaterials represent an emerging class of man-made artificially structured materials whose properties do not come from their chemical composition, but from the way the material is arranged in space, which can be described by the so-called representative unit cell. The influential concept of metamaterials was first introduced in a paper by Bose [1], who described an artificial twisting structure that had an impact on the rotation of the polarisation plane of electromagnetic waves. While the term *metamaterial* is often associated with optical and electromagnetic applications, it also includes mechanical metamaterials (MMs). Metamaterials possess huge potentialities in creating materials whose properties go beyond those usually found in standard materials, and some counterintuitive properties can be achieved such as: negative stiffness [2–5], tunable thermal conductivity [6,7], negative Poisson's ratio (*auxetic* materials) [8–13], negative refractive index [14,15], negative permeability [16], tailorable defect tolerance [17], and multistability [18–23], to mention a few. Thanks to their unusual properties, to date, metamaterials find significant and various applications in aerospace engineering, medicine, defense technology, electronics, as well as robotics, and in many other application fields [24–27]. Such materials, freeing themselves from the constraints

of natural material properties, are pushing the boundaries of functional design and driving the advancement of novel materials. They are at the forefront of ongoing material research, offering new avenues for exploration and progress.

Soft polymers are extensively utilised in the production of compliant metamaterials, with 3D printing being a well-established method for their fabrication [28]. However, despite advancements in the manufacturing technology, defects still occur in printed parts, significantly impacting their quality. These defects can manifest themselves in both the geometry and the base material, exerting a strong influence on the overall performance of the printed object. Unintentional defects introduced during manufacturing can lead to compromised performance, necessitating careful consideration during the design phase. While previous research has predominantly focused on defect sensitivity in metallic and brittle lattice structures [29–31], assessing the impact of 3D printing-induced defects on soft lattice metamaterials remains quite unexplored. This topic holds significant importance, particularly within the emerging field of 3D printed soft robotic materials [32–34]. Moreover, since in this work we study the influence of defects on the mechanical behaviour of lattice structures both at small and high strains, ductile materials are needed. Unfortunately,

\* Corresponding author.

E-mail address: [andrea.spagnoli@unipr.it](mailto:andrea.spagnoli@unipr.it) (A. Spagnoli).

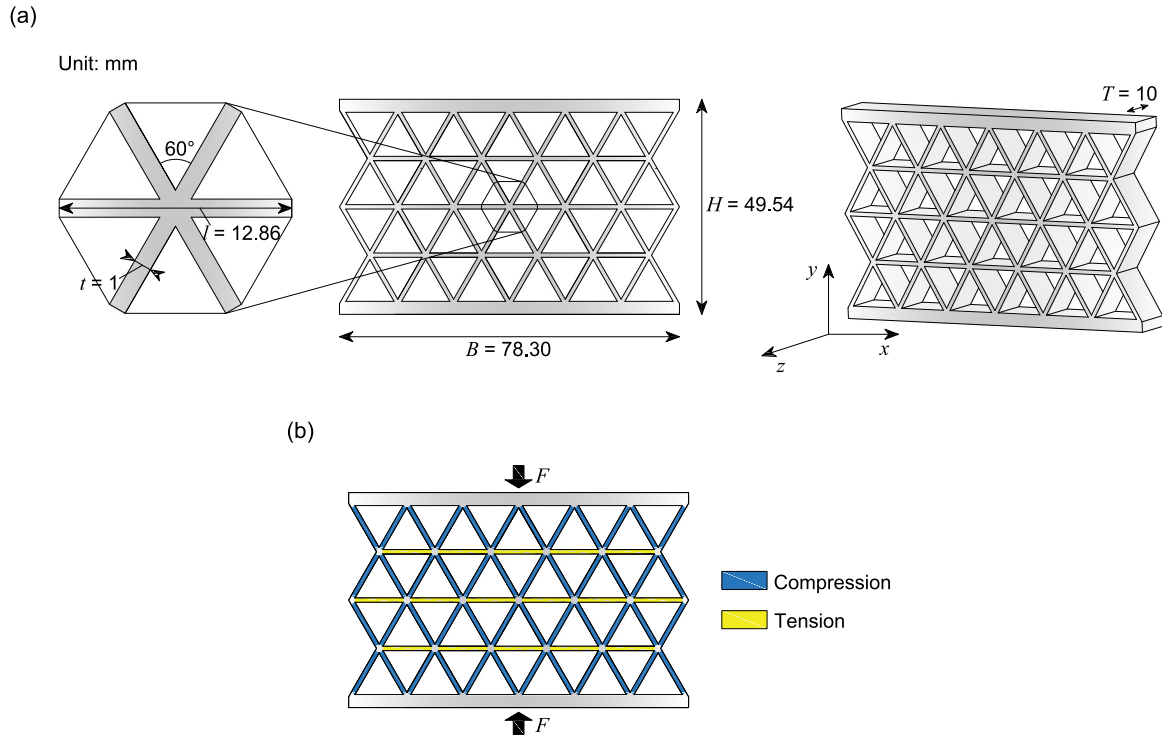


Fig. 1. (a) Geometrical dimensions of the considered lattice structure. (b) Stress conditions arising in the lattice structure undergoing compressive loading.

employing metallic 3D printers would not align with our goals, since they produce stiff and quite brittle objects. For this reason, we make use of the FDM technology for manufacturing all the specimens, employing a flexible filament material.

A multiphase material, as defined in Ref. [35], refers to an object that combines two or more materials in an organic and synergistic manner, as opposed to a single-phase material that only uses one type of material for construction. As a result, the popularity and development of multiphase materials and structures have grown significantly. Despite this increasing popularity, the field of multiphase MMs is still in its early stage, with limited research conducted, primarily due to significant challenges that demand manufacturing and modelling refinement and resolution. These materials and structures have the ability to expand the design space and provide improved solutions, making it possible to effectively leverage different materials to their fullest potential. Recently, multiphase solid cellular structures have extensively been studied to obtain enhanced mechanical performances [36–48]. However, the strategy of employing a secondary incompressible material for mitigating the defect sensitivity of lattice metamaterials has not been explored yet.

Here, we consider a classical 2D metamaterial whose architecture consists in a lattice periodic structure made of regular triangular cells. The mechanical response of such a lattice structure under compressive load appears to be characterised by a local buckling phenomenon taking place in the compressed elements, which significantly reduces the mechanical performances of the structure both at small and large strains. From the above consideration, it clearly appears that the presence even of small defects promoting the appearance of local instabilities, can greatly reduce the load bearing capacity of such structures and a way of reducing such a drawback is highly desirable. Investigating this reduction through the use of partial filling with an incompressible material is the main goal of the present work.

## 2. Design and methods

### 2.1. Lattice design

In this work, we focus our attention on the most classical 2D stretch-dominated (in which the beams are characterised by tensile or compressive forces in their trivial configuration of equilibrium) lattice geometry [49]. In particular, the considered structure is made of  $11 \times 4$  regular triangular cells (for a total of 64 beams) with overall dimensions  $B \times H \times T = 78.3 \times 49.5 \times 10$  mm and characterised by beam elements whose sizes are equal to  $l \times t \times T = 12.86 \times 1 \times 10$  mm (Fig. 1a). The resulting relative density of the metamaterial is equal to  $\rho = V^*/V_s = 0.32$ , where  $V^*$  is the volume of the lattice ( $12,343.18 \text{ mm}^3$ ) and  $V_s$  is the volume of the solid core with identical thickness ( $B \times H \times T = 38,758.5 \text{ mm}^3$ ). Stress conditions arising in the elements of the lattice structures under a compressive loading are depicted in Fig. 1b.

### 2.2. Imperfection types

Geometrical imperfections are introduced to study the sensitivity of the mechanical response of the lattice structure to the presence of defects. The role of such imperfections on the mechanical behaviour consists in promoting the appearance of local instabilities of some elements with a consequent reduction of the overall load bearing capacity of the structure. Three different types of geometric anomalies have been defined, namely: (1) curvature (whose amount is defined by a lateral shift of the beam element's midpoint equal to  $v = 0.1 l$ , Fig. 2a) attributed to some of the elements constituting the lattice; (2) lateral shift  $s$  of some nodes of the lattice ( $s = \pm 0.1 l$ , Fig. 2b); (3) reduced thickness of the beam elements ( $t_r = 0.9 t$ , Fig. 2c).

The three types of imperfections have been introduced randomly in the 2D structure (Fig. 3).

For the beam curvature and width defects, 6 beams are affected by such imperfections (corresponding to a 9.4% of defective beams in the

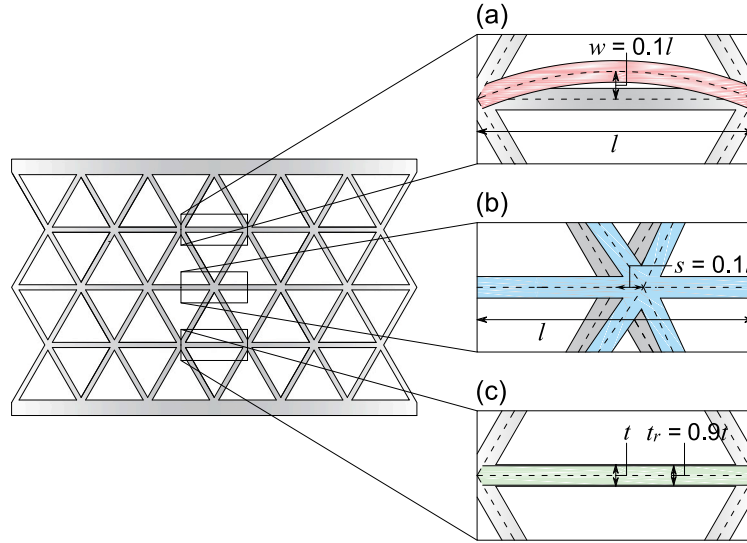


Fig. 2. Geometrical imperfections: beam curvature (a), node shifting (b), beam width (c).

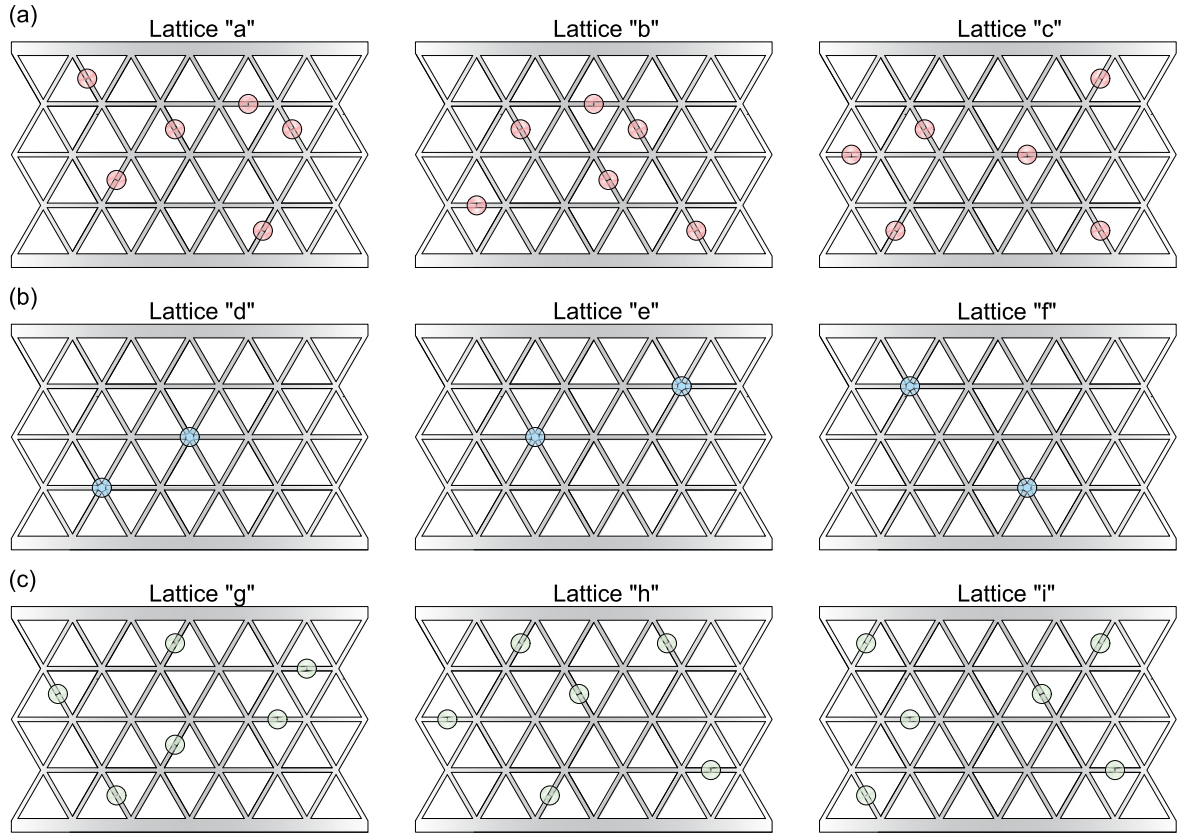


Fig. 3. Locations of the randomly generated geometrical imperfections and lattices ID. Imperfection type: (a) beam curvature, (b) node position, (c) beam width.

structure). On the other hand, for the node shifting case, 12 beams are interested (corresponding to a 18.8% of defective beams).

### 2.3. Manufacturing of two-phase lattice metamaterials

All the designed lattice structures, after being generated with the CAD software Onshape, are converted into stereolithographic (STL) format and then sliced with ideaMaker slicer. The lattice structures, made of a commercially available thermoplastic polyurethane (TPU)

material (Cheetah by NinjaTek) in the shape of a filament with a nominal diameter of 1.75 mm, are obtained by using a FDM 3D printer Raise3D E2. Firstly, the 3D printer is calibrated using a Z-probe to determine the exact distance between the nozzle tip and the print bed. Then, a bed leveling process is carried out to ensure a flat and stable print bed without any rotation or tilting. The detailed printing parameters are listed in Table 1.

The building direction is set along the direction [0 0 1] (see Fig. 1a). In order to create a bi-material structure, both empty and filled lattices

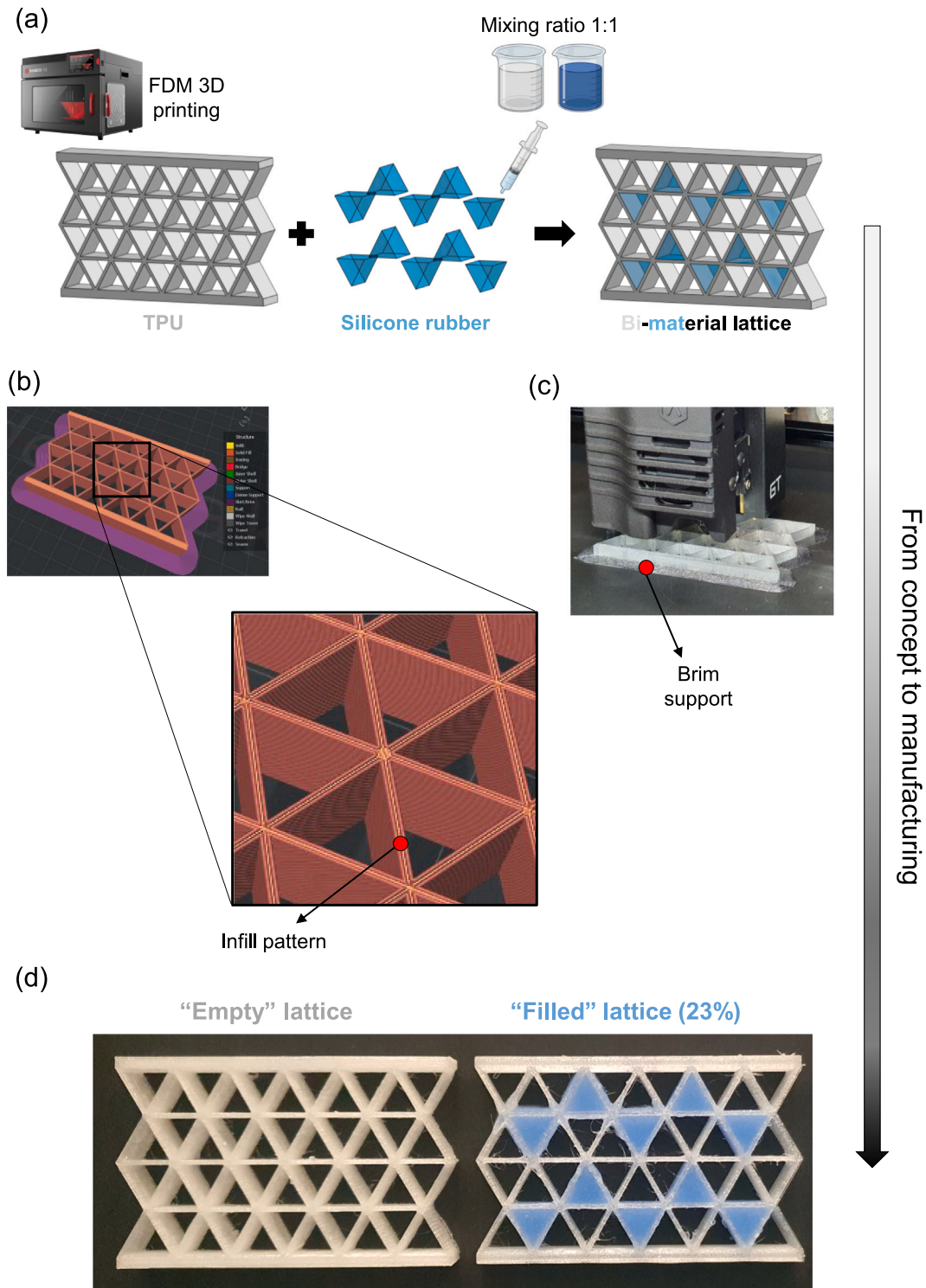


**Fig. 4.** (a) Schematic of the manufacturing process of the bi-material lattice structures. (b) Filament printing path of the 3D printed specimens. (c) View of a lattice during the printing process. (d) Pictures of an *empty* lattice and a lattice with a fixed pattern of filled cells (*filled* lattice), respectively.

are considered; in the latter case, a regular filling pattern is considered as shown in Fig. 4a. The filling material consists of Bluesil RTV 3619 A and B by Elkem, poured in the single cells until they are completely filled. The Bluesil RTV 3619 A and B is a two component (base + catalyst) incompressible silicone elastomer which cures at room temperature by a polyaddition reaction in a 1:1 mixing ratio (Fig. 4a). No adhesive is used between the silicone and the lattices. It is important to note that the filling pattern is kept the same for all the specimens,

irrespectively of the presence of defects, and of their type and location. Thicker upper and lower side of the specimens are designed to avoid the irregular deformation of the TPU at both ends of the lattice. The manufacturing process of the lattice structures is summarised in Fig. 4a and pictures of an empty and partially filled lattice are shown in Fig. 4b. During the fabrication process, it is determined that considering the warping of samples is crucial when setting up the print. Inadequate support during printing results in the warping of the TPU material due



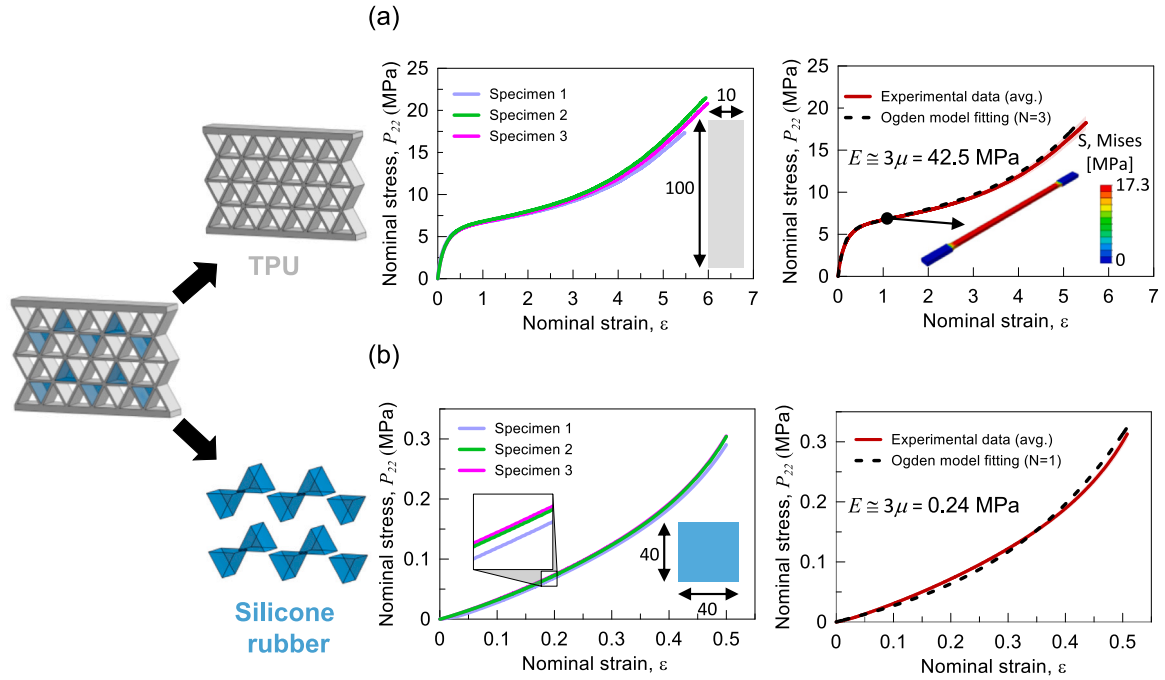


Fig. 5. Mechanical characterisation of the constituent materials. All the samples are tested at a nominal strain rate of  $0.002 \text{ s}^{-1}$ . (a) Dimensions (mm) of the tensile TPU specimens and 3rd order Ogden model fitting of the experimentally obtained average stress–strain curve. The inset image shows the numerically derived Von Mises stress distribution in a tensile specimen at 109% axial strain. (b) Dimensions (mm) of the cubic silicone specimens and 1st order Ogden model fitting of the experimentally obtained average stress–strain curve.

Table 1  
Printing parameters.

Parameter	Value
Layer height	0.2 mm
Infill density	100%
Extrusion width	0.32 mm
Nozzle temperature	235 °C
Printing platform temperature	70 °C
Printing speed	30 mm/s

Table 2  
Material properties employed in the numerical simulations.

ID	$\mu_i$ (MPa)	$\alpha_i$ (–)	$\rho$ (g/cm <sup>3</sup> )
TPU	–11.40	3	1.18
	3.26	3.42	
	22.5	–5.11	
Silicone	0.08	7.59	1.05

to residual stresses arising from the cooling process. In order to prevent this issue, it is decided to print all the lattices with a brim support all along the lattice borders (Fig. 4a). After completing the printing process, the TPU supports are meticulously removed using fine tweezers. Six lattices for each type of imperfections are fabricated (3 empty and 3 filled), for a total of 18 *defective* lattices. In addition, we fabricate 6 additional lattices (3 empty and 3 filled) without imperfections. One specimen is printed for each resulting configuration.

### 3. Experimental tests and FE validation

The mechanical tests include tensile and compression tests for the characterisation of the bulk mechanical properties of the TPU and the silicone, respectively, and compression tests for evaluating the in-plane compression behaviour of the two-phase lattice metamaterials.

All the mechanical tests are performed by using a universal testing machine Galdabini Quasar 2.5, equipped with a 3 kN load cell, with computer control and data acquiring system, at a room temperature of 20 °C. Pictures are taken by means of a Basler acA5472-17uc USB 3.0 camera. The specimens are left on the printing bed for a specific duration, allowing for a gradual and controlled decrease in temperature of the lattice so as to avoid thermal distortions in the lattice itself. To ensure consistency across all experiments, all specimens have been tested exactly 24 h after manufacturing. This approach guarantees that the temperature variation experienced by the lattices remains constant for all the specimens.

#### 3.1. Mechanical characterisation of the constituent materials

A preliminar series of tests are conducted in order to analyse the mechanical properties of the bulk materials. Three  $10 \times 150 \times 4 \text{ mm}^3$  TPU rectangular specimens are 3D printed with a 100% density and  $\pm 45^\circ$  rectilinear infill pattern and tensile tested until rupture at a strain rate of  $0.002 \text{ s}^{-1}$ , while compression tests under displacement controlled mode are performed on three  $40 \times 40 \times 40 \text{ mm}^3$  cubic silicone specimens at the same strain rate. This low strain rate is employed in order to have quasi-static conditions. The results of the mechanical characterisation are reported in Fig. 5, along with the fitting curves using an incompressible Ogden strain energy function for both TPU and silicone

$$\Psi = \sum_{i=1}^N \frac{2\mu_i}{\alpha_i^2} (\lambda_1^{\alpha_i} + \lambda_2^{\alpha_i} + \lambda_3^{\alpha_i} - 3) \quad (1)$$

where  $\lambda_1, \lambda_2, \lambda_3$ , are the principal stretches and  $\mu_i, \alpha_i$ , are material constants.

The response of TPU and silicone is described by an Ogden model with  $N = 3$  and  $N = 1$ , respectively. A summary of the material parameters employed to perform the FE analyses is given in Table 2.

#### 3.2. Compressive response of lattice metamaterials

As shown in Fig. 6, it is expected that each lattice structure under compression will undergo three distinct regions: initial linear elastic

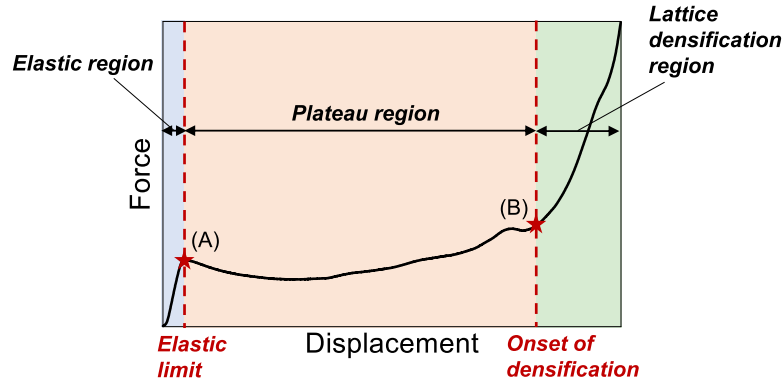


Fig. 6. Typical force–displacement curve for the compression regions of lattice structures. The points indicated by a red star in the plot correspond to the compressive strength (A) and the compressive stress at 50% strain (B), respectively.

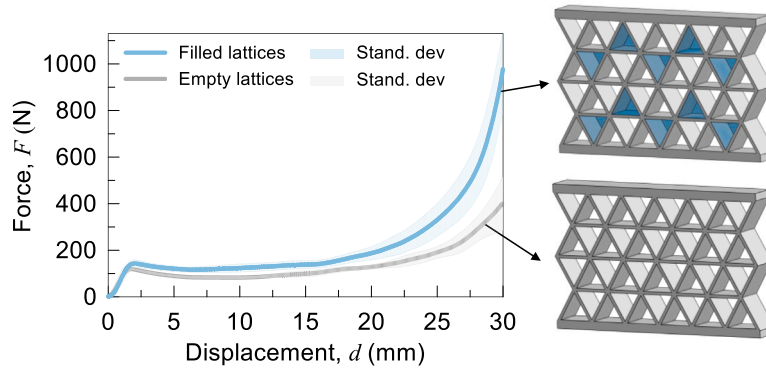


Fig. 7. Preliminary investigation of the silicone's filling effect on the mechanical behaviour of the lattices without imperfections.

deformation, succeeded by a plateau involving plastic deformation and a final densification, in which a dramatic and continuous increase in the load occurs, tending the structure to behave as the constituent material [49].

Upon completion of the compression tests, the following parameters are evaluated to analyse and compare the mechanical behaviour of the tested structures: compressive strength, compressive stress at 50% strain, energy absorption ( $EA$ ), and specific energy absorption ( $SEA$ ). The compressive strength of the lattice structure is defined as the first local peak in the stress–strain curve, indicating the initiation of plastic deformation. Next, in order to evaluate the improvement in the load bearing capacity of the structure at high deformations, it is decided to track the compressive stress related to an overall applied 50% strain (corresponding to an applied displacement of the loading plate  $d = 25$  mm). Finally, the energy absorbing capacity and specific energy absorption of lattice structures play a crucial role as key performance indicators, particularly in weight-bearing applications. These indicators are calculated at 50% compressive strain [12]. The energy absorbed by the lattice ( $EA$ ) is equal to the integral of the force–displacement curve,

$$EA = \int_0^d F(\delta) d\delta \quad (2)$$

The specific energy absorption ( $SEA$ ) provides an indicator of the energy absorbed per unit mass ( $m$ ), that is:

$$SEA = \frac{EA}{m} \quad (3)$$

### 3.3. Results on the perfect lattices

A preliminar investigation is conducted through ramp-shaped mechanical tests with a displacement speed equal to  $5 \text{ mm min}^{-1}$ , until densification is reached. The sampling frequency of all the measured

quantities is set to 5 Hz. During the tests no out-of-plane displacements are observed. As a first step, in order to highlight the silicone's filling effect on the mechanical performances of the lattices, we conduct compression tests on lattices without imperfections using the fabricated 3 empty lattices and 3 filled lattices. The obtained force–displacement curves are shown in Fig. 7. Note that, due to the incompressible behaviour of silicone, the filled cells tend to maintain their initial area during the lattice's deformation, at least as long as no detachment between TPU and silicone occurs.

Table 3 reports the values of the relevant mechanical parameters analysed for each type of lattices. To determine stress values for each scenario, the load is divided by the cross-sectional area of the lattice structure perpendicular to the loading direction ( $B \times T$ , see Fig. 1a). Additionally, strain values are calculated by dividing the displacement,  $d$ , by the height of the lattice structure ( $H$ , see Fig. 1a).

From the experimental data, it is possible to determine that the silicone filling of the structure causes an average increase of +18%, +71%, 42%, and 5% of compressive strength, compressive stress at 50% strain, energy absorption and specific energy absorption, respectively (see Table 3).

#### 3.3.1. Finite element validation

The commercial FE software ABAQUS/CAE [50] is employed to numerically investigate the mechanical behaviour of the lattices. The Dynamic/Explicit module is used for all the simulations, in order to manage large deformations and complex contacts. The lattice geometry is imported as a STEP file format. Two discrete rigid plates are set on the bottom and top of the lattice structures to simulate the actual experimental conditions and are fixed to the lattices by employing a tie constraint. Load and boundary conditions are defined at the top and bottom reference points: the lower plate is fixed while a displacement,  $d$ , of 30 mm (corresponding to a 60% nominal strain) is imposed to

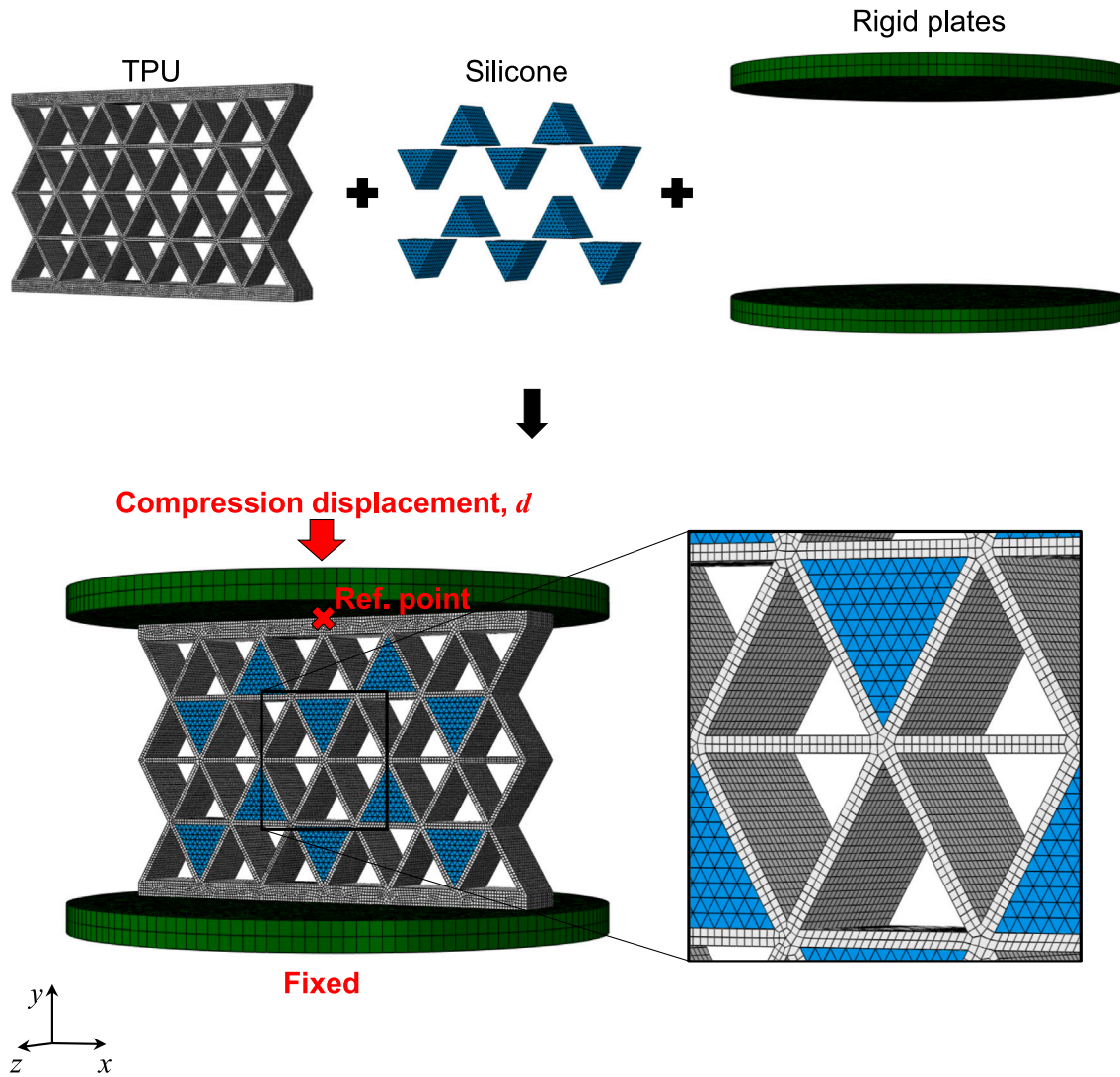


Fig. 8. FE model of a partially filled lattice and detailed view of the mesh employed.

Table 3

Experimental data obtained from the compressive tests on empty and filled lattices without imperfections.

Lattice material	Sample	Compressive strength, (MPa)	Compressive stress at 50% strain, (MPa)	Energy absorption, (J)	SEA, (J/g)
TPU	1	0.152	0.216	2.502	0.170
	2	0.163	0.226	2.698	0.183
	3	0.151	0.274	2.687	0.182
	<b>Avg</b>	$0.155 \pm 0.01$	$0.239 \pm 0.03$	$2.629 \pm 0.11$	$0.178 \pm 0.01$
TPU + silicone	1	0.199	0.445	4.024	0.202
	2	0.194	0.473	4.062	0.204
	3	0.159	0.308	3.139	0.158
	<b>Avg</b>	$0.184 \pm 0.02$ (+18%)	$0.409 \pm 0.09$ (+71%)	$3.742 \pm 0.52$ (+42%)	$0.188 \pm 0.03$ (+5%)

the top plate in order to study the behaviour of the structure at large deformations. The mechanical response of the TPU and the silicone has been modelled with an Ogden's hyperelastic material model with  $N = 3$  and  $N = 1$ , respectively (see Table 2). During the analysis process, a general contact algorithm is employed: the tangential friction coefficient is set as 0.2 while hard contact is adopted in the normal direction. Eight node brick elements with reduced integration (C3D8R) are used for the discretisation of the geometry of the TPU, 6-node triangular prism elements (C3D6R) with reduced integration are employed for the silicone, and three-dimensional rigid elements (R3D4) are used for the two plates. A maximum mesh size equal to 0.50 mm, 1 mm, and 2 mm is employed in all the subsequent analyses for the TPU, the silicone, and the rigid plates, respectively. Further mesh refinements

do not improve significantly the results. Hence, the FE models of the empty and filled lattice are discretised with 113,638 and 162,592 finite elements, respectively. The force  $F$  is obtained by acquiring the reaction force on a reference point tied to the upper plate during the simulation. The FE models for a partially filled lattice is shown in Fig. 8.

In order to minimise computational expenses, the explicit solver's stable time is reduced using the mass-scaling technique. Although this adjustment reduces the overall simulation duration, it results in higher inertial forces. To ensure that the loading remains in the quasi-static conditions, the kinetic energy is verified to be less than 5% of the internal energy of the structure throughout the entire deformation process [50] (Fig. 9).

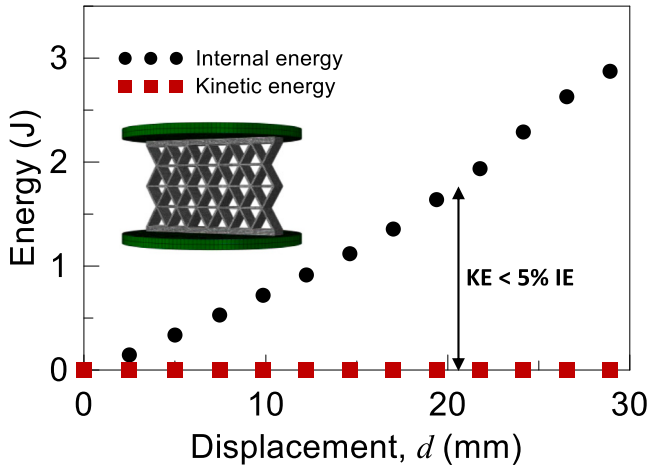


Fig. 9. Comparison between the internal energy and the kinetic energy for a FE analyses on an empty lattice, proving the assumption of a quasi-static phenomenon. Similar results are obtained for the filled lattice.

The comparison between the numerically and experimentally obtained force–displacement curves of the lattices is shown in Fig. 10a. Despite some discrepancies in the values of the loads at low levels of strains, a good agreement can be observed between numerical and experimental results for the three stages of the force–displacement curve: linear elastic, plastic collapse plateau and the final densification. It is demonstrated that the silicone filling improves the load bearing capacity of the structures. Moreover, in Fig. 10b, a good comparison can be also observed from the values of the energy absorbed at different strains (10%, 20%, 30%, 40%, 50%). Finally, the experimental and numerical deformation shapes seem to match quite well (Fig. 11a and Fig. 11b).

#### 3.4. Results on the defective lattices

Next, we draw our attention to the defective lattices. Fig. 12 shows the comparison between the experimentally obtained force–displacement curves of the empty and partially filled defective lattices, for each type of geometrical imperfections. For the sake of completeness, the average curves for lattices without geometrical anomalies are also reported.

As expected, it is observed that all the lattices go through an elastic, a plateau, and a densification stage. During the elastic stage, the force

increases linearly with the increasing of displacement and the stiffness of the silicone-filled lattices is similar to that of the empty lattices. This is due to the low Young's modulus of the silicone ( $E = 0.24$  MPa) and the low silicone filling percentage ( $\sim 23\%$ ). During both the plateau and the densification stages, the measured forces of the silicone-filled lattices are much higher than those of the empty lattices, thanks to the severe hardening of the silicone at high strains. Finally, it is worth stating that the defects play a major role even in the plastic region after the first peak load, reducing the load bearing capacity of the structures.

#### 4. Discussion

Here we summarise the overall results obtained by the uniaxial compressive tests on the lattice metamaterials. In Fig. 13 the compressive strength, compressive stress at 50% strain, energy absorption and specific energy absorption for the defective empty and filled lattices are shown. Moreover, for estimating the capability of the silicone filling to compensate the geometrical imperfections introduce in the structures, the average value of each parameter considered for the lattices with no imperfections is reported.

For the sake of completeness, Tables 4 and 5 show all the experimentally obtained values of the mechanical parameters of interest for all the lattices.

From the analysis of the results, it can be determined that the introduction of the imperfections in the structure of the lattices causes an average decrease of  $-19\%$ ,  $-28\%$ ,  $-20\%$ ,  $-9\%$  in the compressive strength, compressive stress at 50% applied strain, energy absorption ( $EA$ ) and specific energy absorption ( $SEA$ ), respectively, with respect to the *perfect* empty lattices. Moreover, it also turns out that the worst geometrical defect is the reduced beam thickness. On the other hand, even adding a small constant amount of a secondary soft material in a specific filling pattern significantly improves the mechanical behaviour of the lattices. In particular, a percentage difference of  $-3\%$ ,  $+37\%$ ,  $+21\%$ ,  $-6\%$  (positive values correspond to an average increase of the relevant parameter with respect to the baseline case) with respect to the *perfect* empty lattices is obtained, almost compensating the presence of any type of imperfections.

#### 5. Conclusions

The present paper provides insights into the mechanical behaviour of two-phase 3D printed lattice metamaterials subject to uniaxial compression and strategies for mitigating their defect sensitivity. In particular, the most classical configuration characterised by regular triangular unit cells has been investigated. After the mechanical characterisation of the primary material of the lattice structures, a thermoplastic

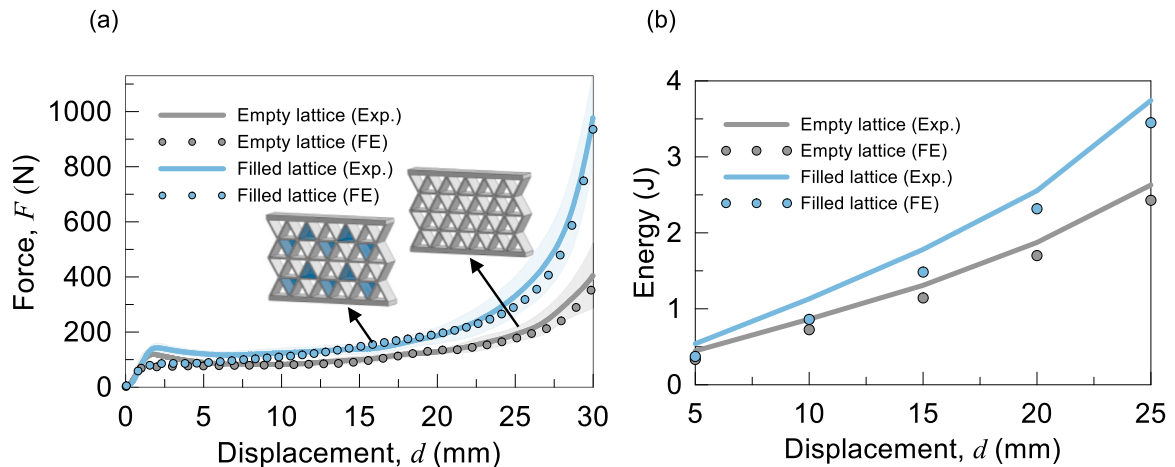


Fig. 10. (a) Comparison between the experimental and numerical force–displacement curves of an empty and filled perfect lattice under uniaxial compression along the  $y$ -direction. (b) Comparison between the experimentally and numerically obtained energy absorbed of an empty and filled perfect lattice. Compressive strain ranges from 10% to 50%.



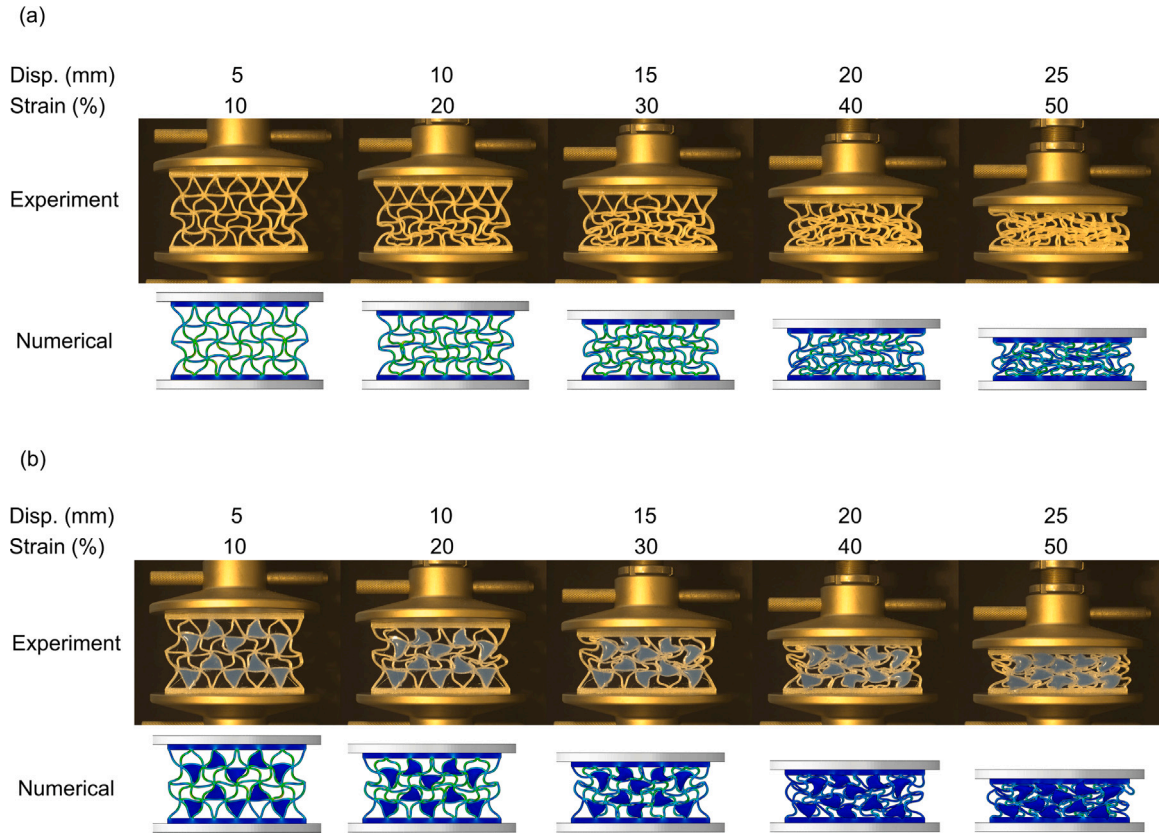


Fig. 11. Comparison between numerical and experimental deformed configurations at different strains (10%, 20%, 30%, 40%, 50%) for an empty (a) and filled (b) perfect lattice.

Table 4

Experimental data obtained from the compressive tests on empty defective lattices.

Type of imperfection	Lattice ID	Compressive strength, (MPa)	Compressive stress at 50% strain, (MPa)	Energy absorption, (J)	SEA, (J/g)
Beam curvature	a	0.139	0.203	2.433	0.171
	b	0.139	0.179	2.469	0.172
	c	0.148	0.225	2.451	0.173
Node shifting	d	0.126	0.165	2.027	0.154
	e	0.125	0.185	2.112	0.160
	f	0.139	0.197	2.254	0.173
Beam width	g	0.110	0.176	1.911	0.148
	h	0.126	0.159	2.014	0.155
	i	0.128	0.208	2.060	0.161
	<b>Avg</b>	$0.131 \pm 0.01$	$0.189 \pm 0.02$	$2.192 \pm 0.21$	$0.163 \pm 0.01$

Table 5

Experimental data obtained from the compressive tests on filled defective lattices.

Type of imperfection	Lattice ID	Compressive strength, (MPa)	Compressive stress at 50% strain, (MPa)	Energy absorption, (J)	SEA, (J/g)
Beam curvature	a	0.168	0.377	3.655	0.188
	b	0.158	0.366	3.619	0.186
	c	0.156	0.404	3.567	0.180
Node shifting	d	0.151	0.275	3.017	0.158
	e	0.149	0.293	3.063	0.159
	f	0.149	0.372	3.192	0.178
Beam width	g	0.126	0.274	2.644	0.139
	h	0.147	0.290	3.038	0.162
	i	0.139	0.300	2.970	0.163
	<b>Avg</b>	$0.149 \pm 0.01$	$0.328 \pm 0.05$	$3.196 \pm 0.35$	$0.167 \pm 0.01$

polyurethane, and the secondary *reinforcing* material, a commercially available silicone rubber, several 2D lattice samples are designed and additively manufactured. Geometrical imperfections are introduced to evaluate the sensitivity of the mechanical behaviour of the lattice structure to the presence of intrinsic defects whose role consists in promoting the appearance of local instabilities of some elements with

a consequent reduction of the load bearing capacity, both at small at high strain regimes. All the specimens (bare lattice structures and silicone-filled composites) are experimentally tested under quasi-static compression. FE analyses are performed in order to verify the experimentally obtained improvement in the mechanical response of the structures caused by the silicone filling. The overall trend of the

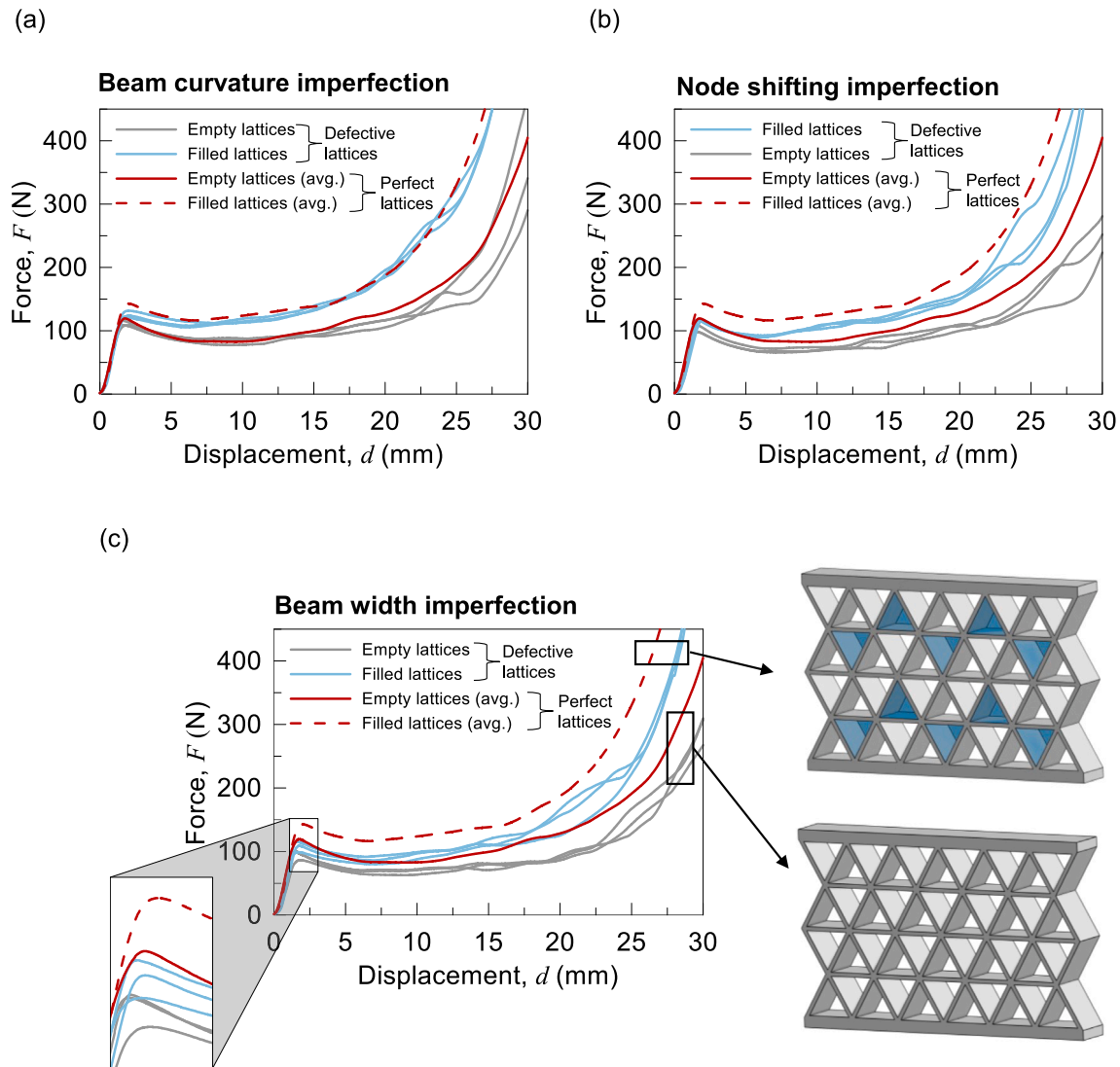


Fig. 12. Experimentally obtained force-displacement curves, for empty and partially filled lattices, for the beam curvature imperfection (a), node position imperfection (b), and beam width imperfection (c).

compressive behaviour of such structures seems to be captured pretty well by the FE models even at severe applied deformations. The difference between experiments and simulations in the first peak load might be attributed to the influence of the infill pattern during 3D printing on the buckling of beam elements (Fig. 4b) [51,52]. Such a pattern is not described in the FE models, where the TPU is treated as an homogeneous material. From the analysis of the experimental results, it turns out that the introduction of the imperfections in the structure of the lattice causes an average decrease of  $-19\%$ ,  $-28\%$ ,  $-20\%$ ,  $-9\%$  in the compressive strength, compressive stress at 50% applied strain, energy absorption ( $EA$ ) and specific energy absorption ( $SEA$ ), respectively, with respect to the *perfect* empty lattices. On the other hand, adding a secondary soft material in a specific filling pattern significantly improves the mechanical behaviour of the lattices. In particular, a percentage difference of  $-3\%$ ,  $+37\%$ ,  $+21\%$ ,  $-6\%$  with respect to the *perfect* empty lattices is obtained, almost compensating the presence of imperfections. The present investigation provides useful insights into the strength of soft multimaterial lattice structures, offering a strategy of employing a secondary material in order to mitigate

the defect sensitivity of such metamaterials. These findings could be used in the development of novel light weight functional structures.

#### CRediT authorship contribution statement

**Matteo Montanari:** Conceptualization, Methodology, Visualization, Investigation, Writing – original draft. **Roberto Brighenti:** Conceptualization, Writing – review & editing. **Andrea Spagnoli:** Conceptualization, Writing – review & editing, Supervision.

#### Declaration of competing interest

The authors declare that they have no known competing financial interests or personal relationships that could have appeared to influence the work reported in this paper.

#### Data availability

Data will be made available on request.

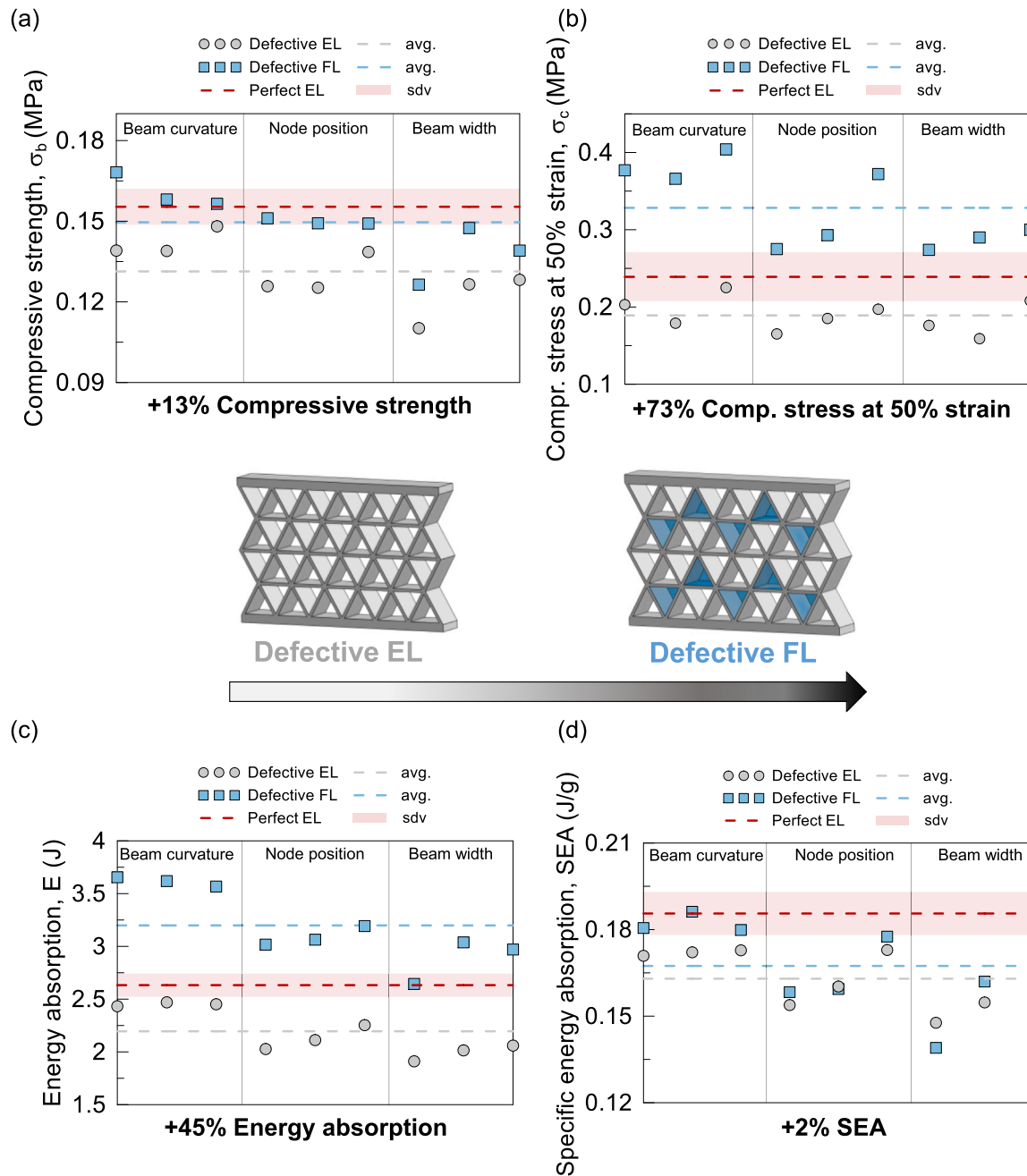


Fig. 13. Comparison between the experimentally obtained compressive strength (a), compressive stress at 50% strain (b), energy absorption (c) and specific energy absorption (d) for the empty lattice (EL) and for the (partially) filled lattices (FL), for each type of geometrical imperfections. For the sake of completeness, the average value and the standard deviation of each parameter considered for the lattice structures with no imperfection is highlighted in red.

## References

- [1] Bose JC. On the rotation of plane of polarisation of electric wave by a twisted structure. *Proc R Soc London* 1898;63(389–400):146–52.
- [2] Tan X, Chen S, Wang B, Tang J, Wang L, Zhu S, et al. Real-time tunable negative stiffness mechanical metamaterial. *Extreme Mech Lett* 2020;41:100990.
- [3] Zhang K, Qi L, Zhao P, Zhao C, Deng Z. Buckling induced negative stiffness mechanical metamaterial for bandgap tuning. *Compos Struct* 2023;304:116421.
- [4] Xiao L, Bursi OS, Wang M, Nagarajaiah S, Sun F, Du X-L. Metamaterial beams with negative stiffness absorbers and rotation: band-gap behavior and band-gap merging. *Eng Struct* 2023;280:115702.
- [5] Li Q, Yang D, Ren C, Mao X. A systematic group of multidirectional buckling-based negative stiffness metamaterials. *Int J Mech Sci* 2022;232:107611.
- [6] Brighenti R, Tatar F. Thermo-mechanical performance of two-dimensional porous metamaterial plates. *Int J Mech Sci* 2023;238:107854.
- [7] Cai J, Estakhrianhaghghi E, Akbarzadeh A. Functionalized graphene origami metamaterials with tunable thermal conductivity. *Carbon* 2022;191:610–24.
- [8] Tan X, Chen S, Wang B, Tang J, Wang L, Zhu S, et al. Real-time tunable negative stiffness mechanical metamaterial. *Extreme Mech Lett* 2020;41:100990.
- [9] Peng X-L, Bargmann S. Tunable tension–compression asymmetry and auxeticity in lattice structures by harnessing unilateral contact. *Compos Struct* 2021;278:114708.
- [10] Brighenti R, Spagnoli A, Lanfranchi M, Soncini F. Nonlinear deformation behaviour of auxetic cellular materials with re-entrant lattice structure. *Fatigue Fract Eng Mater Struct* 2016;39(5):599–610.
- [11] Ren L, Wu W, Ren L, Song Z, Liu Q, Li B, et al. 3D printing of auxetic metamaterials with high-temperature and programmable mechanical properties. *Adv Mater Technol* 2022;7(9):2101546.
- [12] Zhou J, Liu H, Dear JP, Falzon BG, Kazancı Z. Comparison of different quasi-static loading conditions of additively manufactured composite hexagonal and auxetic cellular structures. *Int J Mech Sci* 2023;244:108054.

- [13] Li Q, Zhan L, Miao X, Hu L, Li E, Zou T. Morning glory-inspired lattice structure with negative Poisson's ratio effect. *Int J Mech Sci* 2022;232:107643.
- [14] Rasad A, Yudistira HT, Qalbina F, Saputro AG, Faisal A. Multilayer flexible meta-materials based on circular shape with negative refractive index at microwave spectrum. *Sensors Actuators A* 2021;332:113208.
- [15] Hien NT, Ca NX, Khuyen BX, Van Huynh T, Khiem NS, Tung NT, et al. Active control of the hybridization effect of near-field coupled resonators in metamaterial for a tunable negative refractive index at terahertz frequencies. *J Phys Chem Solids* 2021;156:110173.
- [16] Di Cesare N, Chamoret D, Domaszewski M. Optimum topological design of negative permeability dielectric metamaterial using a new binary particle swarm algorithm. *Adv Eng Softw* 2016;101:149–59.
- [17] Shaikeea AJD, Cui H, O'Masta M, Zheng XR, Deshpande VS. The toughness of mechanical metamaterials. *Nature Mater* 2022;21(3):297–304.
- [18] Shan S, Kang SH, Raney JR, Wang P, Fang L, Candido F, et al. Multistable architected materials for trapping elastic strain energy. *Adv Mater* 2015;27(29):4296–301.
- [19] Melancon D, Gorissen B, García-Mora CJ, Hoberman C, Bertoldi K. Multistable inflatable origami structures at the metre scale. *Nature* 2021;592(7855):545–50.
- [20] Mao J-J, Wang S, Tan W, Liu M. Modular multistable metamaterials with reprogrammable mechanical properties. *Eng Struct* 2022;272:114976.
- [21] Melancon D, Forte AE, Kamp LM, Gorissen B, Bertoldi K. Inflatable Origami: Multimodal deformation via multistability. *Adv Funct Mater* 2022;32(35):2201891.
- [22] Liang K, Wang Y, Luo Y, Takezawa A, Zhang X, Kang Z. Programmable and multistable metamaterials made of precisely tailored bistable cells. *Mater Des* 2023;227:111810.
- [23] Seyedkanani A, Akbarzadeh A. Magnetically assisted rotationally multistable metamaterials for tunable energy trapping–dissipation. *Adv Funct Mater* 2022;32(52):2207581.
- [24] Lu C, Hsieh M, Huang Z, Zhang C, Lin Y, Shen Q, et al. Architectural design and additive manufacturing of mechanical metamaterials: A review. *Engineering* 2022;17:44–63.
- [25] Zhou X, Ren L, Song Z, Li G, Zhang J, Li B, et al. Advances in 3D/4D printing of mechanical metamaterials: From manufacturing to applications. *Composites B* 2023;254:110585.
- [26] Jiao P. Mechanical energy metamaterials in interstellar travel. *Prog Mater Sci* 2023;137:101132.
- [27] Fan J, Zhang L, Wei S, Zhang Z, Choi S-K, Song B, et al. A review of additive manufacturing of metamaterials and developing trends. *Mater Today* 2021;50:303–28.
- [28] Bikas H, Stavropoulos P, Chrysosolouris G. Additive manufacturing methods and modelling approaches: a critical review. *Int J Adv Manuf Technol* 2016;83(1–4):389–405.
- [29] Seiler P, Tankasala H, Fleck N. The role of defects in dictating the strength of brittle honeycombs made by rapid prototyping. *Acta Mater* 2019;171:190–200.
- [30] El Elmi A, Melancon D, Asgari M, Liu L, Pasini D. Experimental and numerical investigation of selective laser melting–induced defects in Ti–6Al–4V octet truss lattice material: the role of material microstructure and morphological variations. *J Mater Res* 2020;35(15):1900–12.
- [31] Liu L, Kamm P, García-Moreno F, Banhart J, Pasini D. Elastic and failure response of imperfect three-dimensional metallic lattices: the role of geometric defects induced by selective laser melting. *J Mech Phys Solids* 2017;107:160–84.
- [32] Wallin TJ, Pikul J, Shepherd RF. 3D printing of soft robotic systems. *Nat Rev Mater* 2018;3(6):84–100.
- [33] Yap YL, Sing SL, Yeong WY. A review of 3D printing processes and materials for soft robotics. *Rapid Prototyp J* 2020;26(8):1345–61.
- [34] Gul JZ, Sajid M, Rehman MM, Siddiqui GU, Shah I, Kim K-H, et al. 3D printing for soft robotics – a review. *Sci Technol Adv Mater* 2018;19(1):243–62.
- [35] Chen Y, Ye L, Xu C, Zhang Y. Multi-material topology optimisation of micro-composites with reduced stress concentration for optimal functional performance. *Mater Des* 2021;210:110098.
- [36] Zhang XG, Ren X, Jiang W, Zhang XY, Luo C, Zhang Y, et al. A novel auxetic chiral lattice composite: Experimental and numerical study. *Compos Struct* 2022;282:115043.
- [37] Mueller J, Lewis JA, Bertoldi K. Architected multimaterial lattices with thermally programmable mechanical response. *Adv Funct Mater* 2022;32(1):2105128.
- [38] Yavas D, Liu Q, Zhang Z, Wu D. Design and fabrication of architected multi-material lattices with tunable stiffness, strength, and energy absorption. *Mater Des* 2022;217:110613.
- [39] Cheng X, Zhang Y, Ren X, Han D, Jiang W, Zhang XG, et al. Design and mechanical characteristics of auxetic metamaterial with tunable stiffness. *Int J Mech Sci* 2022;223:107286.
- [40] Luo HC, Ren X, Zhang Y, Zhang XY, Zhang XG, Luo C, et al. Mechanical properties of foam-filled hexagonal and re-entrant honeycombs under uniaxial compression. *Compos Struct* 2022;280:114922.
- [41] Mirzaali M, Herranz de la Nava A, Gunashekar D, Nouri-Goushki M, Veeger R, Grossman Q, et al. Mechanics of bioinspired functionally graded soft-hard composites made by multi-material 3D printing. *Compos Struct* 2020;237:111867.
- [42] Usta F, Scarpa F, Türkmen HS, Johnson P, Perriman AW, Chen Y. Multiphase lattice metamaterials with enhanced mechanical performance. *Smart Mater Struct* 2021;30(2):025014.
- [43] Shalchy F, Carlsson J, Deshpande V, Fleck N. Pinching of gel-filled honeycomb. *Int J Solids Struct* 2022;257:111728.
- [44] Günaydin K, Rea C, Kazancı Z. Energy absorption enhancement of additively manufactured hexagonal and re-entrant (auxetic) lattice structures by using multi-material reinforcements. *Addit Manuf* 2022;59:103076.
- [45] Yu R, Luo W, Yuan H, Liu J, He W, Yu Z. Experimental and numerical research on foam filled re-entrant cellular structure with negative Poisson's ratio. *Thin-Walled Struct* 2020;153:106679.
- [46] Novak N, Al-Ketan O, Krstulović-Opara L, Rowshan R, Vesnjak M, Ren Z. Bending behavior of triply periodic minimal surface foam-filled tubes. *Mech Adv Mater Struct* 2022;1–14.
- [47] Prajapati MJ, Kumar A, Lin S-C, Jeng J-Y. Reducing mechanical anisotropy in material extrusion process using bioinspired architected lattice structures. *Addit Manuf* 2023;66:103480.
- [48] Yao R, Pang T, He S, Li Q, Zhang B, Sun G. A bio-inspired foam-filled multi-cell structural configuration for energy absorption. *Composites B* 2022;238:109801.
- [49] Gibson LJ, Ashby MF. Cellular solids: structure and properties. Cambridge solid state science series, 2nd ed.. Cambridge University Press; 1997.
- [50] Dassault Systèmes SIMULIA. Abaqus 2018, Documentation. 2018.
- [51] Lubombo C, Huneault MA. Effect of infill patterns on the mechanical performance of lightweight 3D-printed cellular PLA parts. *Mater Today Commun* 2018;17:214–28.
- [52] Liu W, Song H, Wang Z, Wang J, Huang C. Improving mechanical performance of fused deposition modeling lattice structures by a snap-fitting method. *Mater Des* 2019;181:108065.